nature biotechnology

Discovery of a hepatitis C target and its pharmacological inhibitors by microfluidic affinity analysis

Shirit Einav[1,2,5], Doron Gerber[3,5], Paul D Bryson[2], Ella H Sklan[2], Menashe Elazar[2], Sebastian J Maerkl[3,4], Jeffrey S Glenn[2] & Stephen R Quake[3]

More effective therapies are urgently needed against hepatitis C virus (HCV), a major cause of viral hepatitis. We used *in vitro* protein expression and microfluidic affinity analysis to study RNA binding by the HCV transmembrane protein NS4B, which plays an essential role in HCV RNA replication. We show that HCV NS4B binds RNA and that this binding is specific for the 3′ terminus of the negative strand of the viral genome with a dissociation constant (K_d) of ~3.4 nM. A high-throughput microfluidic screen of a compound library identified 18 compounds that substantially inhibited binding of RNA by NS4B. One of these compounds, clemizole hydrochloride, was found to inhibit HCV RNA replication in cell culture that was mediated by its suppression of NS4B's RNA binding, with little toxicity for the host cell. These results yield new insight into the HCV life cycle and provide a candidate compound for pharmaceutical development.

Over 150 million people are infected with HCV worldwide. Unfortunately, many of these individuals are unable to clear their infection with the current standard of care, which consists of a combination of interferon and ribavirin[1] (Copegus, Rebetol, Rebetron, Virazole). Moreover, this treatment is associated with substantial side effects, precluding its use by many individuals. Thus, current therapies are inadequate for the majority of patients[1], and there is a pressing need for new HCV drugs[1].

The 9.6-kb, positive, single-stranded RNA HCV genome encodes a 3,000-amino-acid polyprotein that is proteolytically processed into structural proteins, which are components of the mature virus, and nonstructural proteins (NS), which are involved in replicating the viral genome[2]. Like other positive-strand RNA viruses[3], HCV appears to replicate in association with intracellular membrane structures. In the case of HCV, the structures are termed the membranous web[4] and are believed to be induced by the NS4B protein. NS4B is also required to assemble the other viral NS proteins within the apparent sites of RNA replication[5]. It is not known how viral RNA, especially the negative-strand template required for production of progeny genomes, might be incorporated or maintained at these replication sites.

NS4B and HCV RNA have been shown to colocalize to the membranous web[6,7], suggesting that NS4B is in intimate contact with viral RNA in the context of authentic viral RNA replication. The hepatitis A and polio picornaviruses have proteins termed 2C, which are required for replication, bind RNA[8,9] and have an N-terminal amphipathic helix and a nucleotide binding motif[8–10]. NS4B contains the same structural features, and both of them are required for HCV replication[5,11]. We thus hypothesized that NS4B may similarly bind RNA, that this interaction might be critical for the HCV life cycle, and that RNA binding by NS4B could be amenable to pharmacologic disruption. To test these hypotheses, we established an *in vitro* RNA binding assay in a format enabling simultaneous analysis of multiple conditions, mutants, replicates, quantitative K_d measurements and high-throughput screening for potential pharmacologic inhibitors.

Like the majority of drug targets[12], NS4B is a membrane protein. Membrane proteins are notoriously difficult to express and characterize biochemically, especially in the quantities required for pharmaceutical screening. Moreover, solubilization by detergents can alter their natural membrane-associated topology. To ameliorate these problems, we used microfluidic tools to perform binding assays with nanoliter protein consumption. This enabled use of an *in vitro* cell lysate expression system, which was supplemented with microsomal membranes to create more natural folding conditions, under which the best NS4B topology data available to date have been obtained[13]. The reduced yield relative to conventional expression methods is offset by low sample consumption.

Previous microfluidic tools to measure drug interactions have been limited to enzymatic targets that can catalyze formation of a fluorescent substrate[14]. In this case we directly measured binding constants by using mechanical trapping of molecular interactions (MITOMI), a microfluidic affinity assay that has previously been used to measure interactions between transcription factors and DNA[15]. We have extended the previous work by showing that MITOMI can be used to measure both binding constants of membrane protein-RNA interactions and inhibition of such interactions by small molecules in a

[1]Department of Medicine, Division of Infectious Diseases and Geographic Medicine, Stanford University School of Medicine, Stanford, California 94305, USA. [2]Department of Medicine, Division of Gastroenterology and Hepatology, Stanford University School of Medicine, CCSR 3115A, 269 Campus Drive, Stanford, California 94305, USA. [3]Department of Bioengineering, Stanford University and Howard Hughes Medical Institute, Stanford, California 94305, USA. [4]Present address: School of Engineering, École Polytechnique Fédérale de Lausanne, Building BM 2111, Station 17, 1015 Lausanne, Switzerland. [5]These authors contributed equally to this work. Correspondence should be addressed to J.S.G. (jeffrey.glenn@stanford.edu) or S.R.Q. (quake@stanford.edu).

Received 30 May; accepted 29 July; published online 31 August 2008; doi:10.1038/nbt.1490

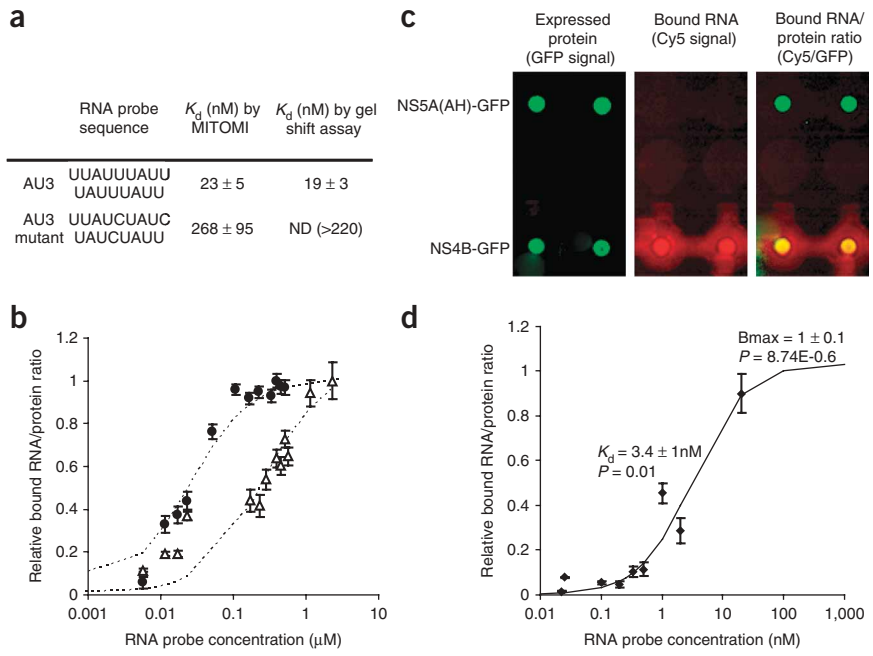

Figure 1 Protein-RNA interactions measured on microfluidic platform. (**a**) Target RNA sequences used to study binding of HuD to RNA and comparison of K_d values measured using microfluidic affinity analysis to values previously measured by gel shift assay[21,22]. ND, not determined. (**b**) Binding curve of HuD to increasing concentration of AU3 (●) and AU3 mutant (△) RNA, as determined in the microfluidic affinity assay. Normalized mean values for 10–20 replicates measured in two independent experiments are shown for each graph. Error bars represent s.d. (**c**) Fluorescent images from microfluidic chip. Left: NS4B-GFP and NS5A(AH)-GFP were anchored to the microfluidic device surface via its interaction with anti-GFP. Middle: an RNA probe corresponding to the 3′ terminal region of the negative viral strand was labeled with Cy5 and incubated with the proteins on the device. Cy5 signal representing bound RNA is shown following a brief wash. Right: an overlay of the Cy5 signal and GFP signal representing bound RNA to protein ratio. (**d**) *In vitro* binding curve of NS4B to serial dilutions of the RNA probe. Each data point represents the mean of 10–20 replicates, and the bars represent the standard error.

high-throughput screen. The latter point was particularly surprising in that the elastomer used to fabricate the device is known to have limitations in chemical compatibility[16,17]; here we show that this does not prevent its use in a drug screen or the discovery of a small molecule with the desired pharmacological properties. Taken together, the results of this paper reveal a novel HCV target and show that microfluidic technology can be used to discover a new pharmaceutical, thereby validating the use of microfluidic tools in drug discovery[18,19].

RESULTS

We validated the use of the microfluidic platform for RNA binding by studying two human proteins from the embryonic lethal abnormal visual system (ELAV) family, the RNA binding activity of which is well characterized[20–22]. We then applied this methodology to study RNA interactions with the transmembrane HCV NS4B protein. We (i) tested the hypothesis that HCV NS4B binds RNA, (ii) determined the K_d for this interaction, (iii) studied the substrate specificity of this binding, (iv) determined the amino acids within NS4B required for RNA binding and (v) screened a compound library for pharmacologic inhibitors of NS4B RNA binding and HCV replication.

Microfluidic assay validation: HuD binding to RNA

HuD is a host cell protein from the ELAV-like family with well-characterized RNA binding activity[20–22]. It is a cytoplasmic protein that contains three conserved RNA recognition motifs through which it binds AU-rich elements in the 3′ untranslated region (UTR) of genes such as those encoding cytokines and proto-oncogenes. Binding was tested against two Cy3-labeled RNA probes: AU3 and a known AU3 mutant to which HuD binding is impaired[21,22] (**Fig. 1**). RNA binding experiments with MITOMI were performed essentially as described[15], except that in this case RNA was used instead of DNA (**Supplementary Fig. 1** online). Briefly, we spotted a microarray of target RNA sequences labeled with Cy3 onto an epoxy-coated slide. These arrays were used to program the microfluidic devices by aligning each spot in the array to a unit cell in the device. After bonding the microfluidic device to a microarray it was subjected to surface patterning that resulted in a circular area coated with biotinylated antihistidine antibodies within each unit cell. The device was then loaded with an *in vitro* transcription-translation mixture containing DNA templates coding for HuD fused in-frame with a C-terminal V5-6 histidine tag (HuD-V5-his) or Gus protein fused in-frame with a C-terminal 6 histidine tag (Gus-his). Bodipy-labeled $tRNA_{Lys}$ was added for protein labeling. Each unit cell was then isolated using micromechanical valves followed by an incubation to allow protein synthesis, binding of the synthesized protein to the surface biotinylated anti-his antibodies, solvation of target RNA and equilibration of proteins and target RNA. MITOMI was then performed by actuation of a 'button' membrane to trap surface-bound complexes while expelling any solution-phase molecules. After a brief wash to remove untrapped, unbound material, the trapped molecules and expressed protein were subsequently detected with an array scanner. The ratio of bound RNA to expressed protein was calculated for each data point by measuring the median signal of Cy3 to the median signal of bodipy.

The assay detected strong binding of HuD to the AU3 RNA probe; background binding by Gus-his was 7- to 16-fold lower than the HuD signal (**Fig. 1a**). This background level did not increase with RNA probe concentration and was subtracted from all chambers (**Supplementary Fig. 2** online). The binding affinity of HuD to the AU3 probe was much greater than that of the AU3 mutant probe: the K_d for AU3 binding was 23 ± 5 nM and that for AU3 mutant binding was 268 ± 95 nM (**Fig. 1a**). These values agree with previous measurements in a gel shift assay[21,22] and validate the MITOMI microfluidic affinity assay for RNA-protein interactions. RNA binding analysis of another protein from the ELAV-like family, HuR, is shown in **Supplementary Fig. 3** online.

NS4B binds HCV RNA and Kd is determined by microfluidics

We then tested whether HCV NS4B binds RNA. Because NS4B is important in viral RNA replication, and initiation of positive-strand RNA synthesis is likely to start at the 3′ terminus of the negative-strand RNA, we first tested binding of NS4B to this region, using a probe designated 3′ negative terminus. A fusion of the amphipathic

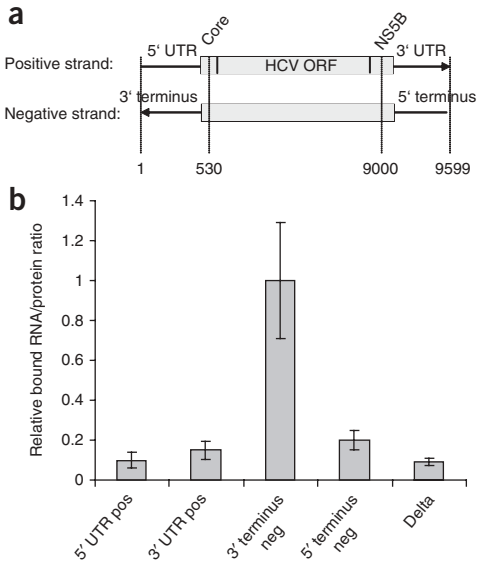

Figure 2 NS4B binds specifically to the 3′ terminus of the HCV negative-strand RNA. (**a**) Four HCV probes were designed. 5′ UTR pos and 3′ UTR pos corresponded to the 5′ UTR and 3′ UTR sequences of the positive viral strand, respectively, and 5′ negative terminus and 3′ negative terminus corresponded to the 5′ and 3′ terminal regions of the negative strand, respectively. The position of these sequences with respect to the HCV open reading frame (ORF) is shown. (**b**) Fractional binding of NS4B to equimolar concentrations of the four HCV probes and to a non-HCV RNA (delta virus RNA) probe. The 3′ terminus of the negative genome strand is favored by > 5×. Each data point represents the mean of 10–20 replicates, and the bars represent the standard error.

helix of NS5A to the N terminus of GFP[5] was used as a negative control. This protein also binds to membranes and can thus anchor the microsomal membranes to the device surface through the interaction of GFP with anti-GFP (**Fig. 1c**). The K_d of NS4B binding to the 3′ terminus of the HCV negative-strand RNA was measured at 3.4 ± 1.0 nM (**Fig. 1d**). To the best of our knowledge this is the first report that HCV NS4B binds RNA. Conventional glutathione-S-transferase (GST) pull-down assays and RNA filter binding assays using recombinant forms of purified NS4B expressed in *Escherichia coli* confirmed this finding (**Supplementary Fig. 4** online), although these were less convenient and amenable to the types of analyses and high-throughput format that we sought.

NS4B specifically binds the 3′ terminus of the (–) viral strand

We measured the substrate specificity of the observed NS4B-HCV RNA interaction with three additional HCV probes (**Fig. 2a**). The probes designated 5′ UTR pos and 3′ UTR pos correspond to the 5′ UTR and 3′ UTR sequences of the positive viral strand, respectively, and 5′ negative terminus corresponds to the 5′ terminus of the negative strand. The RNA binding experiment was repeated and binding of NS4B to equimolar concentrations (3 nM) of the various probes was compared. Whereas NS4B binds all four HCV probes, its apparent affinity to the 3′ negative terminus probe is 5- to 12-fold greater than to the other three HCV RNA regions tested or to an unrelated delta virus RNA genome sequence[23,24] (see **Fig. 2b**). These findings suggest that it is the RNA sequence, and likely the secondary RNA structure, that determines the specificity of NS4B binding to the 3′ terminus of the negative strand.

An ARM in NS4B is essential for RNA binding and HCV replication

Various structural motifs responsible for the interaction between proteins and RNA have been reported[25]. One of these is the arginine rich motif (ARM). ARMs were originally defined as short (10 to 20 amino acids) arginine-rich sequences found in viral, bacteriophage and ribosomal proteins (**Fig. 3a**)[9,25,26]. There is little identity between ARM sequences, other than the preponderance of arginine residues. Subsequently, ARM-like motifs, consisting of longer sequences containing fewer arginines, were identified[9,26]. Inspection of the primary sequence of NS4B reveals the presence of multiple positively charged amino acids (**Fig. 3b**). The majority of these arginine residues are within the last 71 amino acids, in the C-terminal region of NS4B (**Fig. 3b,c**). This region is predicted to form a cytoplasmic segment based on empirical topology studies using glycosylation markers[13]. Elements of this region conform with previously described ARM-like motifs.

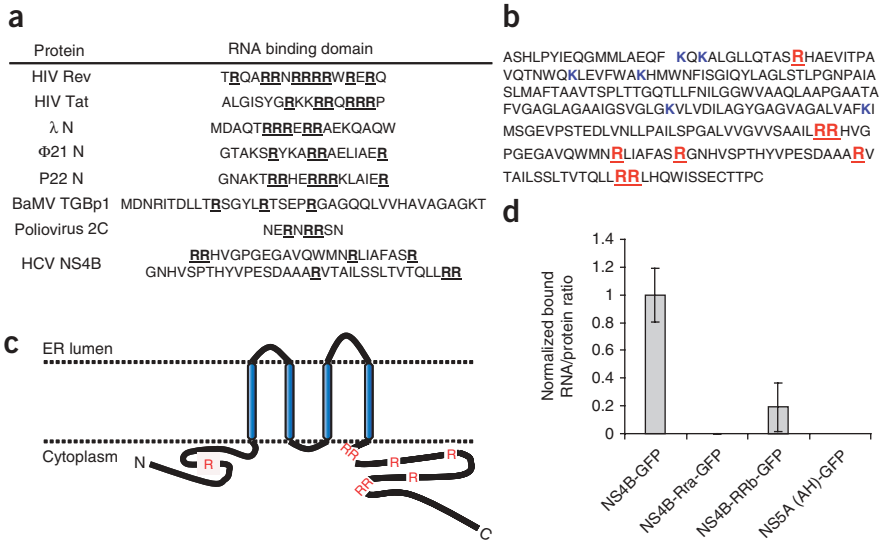

Figure 3 Identification of RNA binding domains within NS4B. (**a**) Arginine-rich sequences known to confer RNA binding found in viral and bacteriophage proteins[9,25,26]. Elements in the terminal loop of NS4B that conform with arginine rich–like motifs are shown at the bottom. Proteins listed are HIV Rev and Tat[25]; λ, Φ21 and P22 bacteriophage antiterminator N proteins[25]; triple gene block protein 1 (TGBp1) of the bamboo mosaic virus (BaMV)[26] and poliovirus 2C[9]. (**b**) Positively charged amino acids (highlighted) within the primary sequence of NS4B (genotype 1a). (**c**) Schematic diagram indicating predicted transmembrane and intracellular domains of NS4B. Conserved positively charged amino acids in the C-terminal segment of NS4B are shown in red. (**d**) Arginine residues mediate RNA binding by NS4B. Binding of wild-type NS4B-GFP, RRa and RRb NS4B-GFP mutants and NS5A(AH)-GFP to the 3′ terminus of the negative viral RNA strand (1.5 nM) was determined by microfluidic affinity analysis. Bars represent s.d.

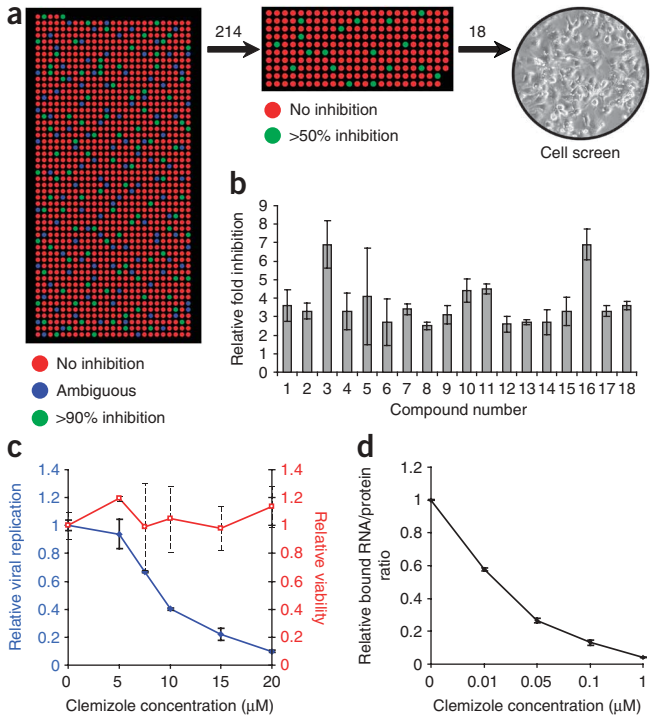

Figure 4 Small-molecule screen reveals that clemizole hydrochloride inhibits RNA binding by NS4B and HCV RNA replication in cell culture. (**a**) The first screen represented a low-stringency measurement of inhibition of 1,280 compounds where the latter were categorized as having high (green), ambiguous (blue) or no (red) inhibition. Based on the initial screen, 214 compounds were then measured again with higher stringency and with a greater number of replicates and the best 18 inhibitors were tested for their ability to inhibit HCV replication via a cellular assay. (**b**) *In vitro* inhibition of NS4B-RNA binding by the top 18 small molecules. (**c**) HCV luciferase reporter–linked cellular assay showing that clemizole inhibits HCV replication (left axis, blue ◆) with no measurable toxicity to the cell as measured by Alamar Blue (right axis, red □). (**d**) *In vitro* NS4B-RNA binding: inhibition curve of clemizole. Each data point represents the mean of 10–20 replicates and the bars represent the standard error.

Using a series of point mutations, we tested if RNA binding by NS4B is mediated by some of its positively charged residues. A substitution of Arg-Arg in positions 192–193 with Ala-Ala was termed 'RRa mutant' and a similar substitution in positions 247–248 was designated 'RRb mutant'. Whereas the RRb mutant decreased binding by NS4B to the 3′ negative terminus probe by fivefold, RNA binding activity to the RRa mutant was completely eliminated at the same probe concentration (1.5 nM; **Fig. 3d**). These results suggest that the tested arginine residues mediate RNA binding by NS4B *in vitro*. To test the hypothesis that these positively charged residues are also important for HCV replication, we introduced these mutations into high-efficiency subgenomic HCV replicons and assayed them in standard replicon colony formation assays (data not shown). The various mutations substantially impaired HCV RNA replication and the degree of replication inhibition correlated with the degree of NS4B RNA binding impairment (unpublished data). These results suggest that efficient binding of HCV RNA is required for viral replication *in vitro*. Alignment of the sequences of natural HCV isolates currently available in databases reveals that these positively charged residues are highly conserved across all HCV genotypes. This conservation suggests that there is a requirement for the RNA binding residues for productive viral infection *in vivo*.

High-throughput screening for inhibitory compounds

We screened a compound library for small molecules that could inhibit the RNA-NS4B interaction. We spotted 1,280 compounds from a small-molecule library on epoxy-coated slides in a microarray format (**Fig. 4a**). The array was allowed to dry and was then aligned and bonded to a microfluidic device. The rest of the assay was performed as before, except that the device was loaded with NS4B-GFP followed by Cy5-labeled 3′ terminus negative RNA probe. In the primary screen, the compounds were spotted at a concentration of ~1 mM. The entire library was screened in duplicate using only two microfluidic devices. Out of 1,280 compounds, 104 were found to have an inhibitory effect (>90% inhibition) on RNA binding by NS4B. In addition, there were 110 compounds for which there was a substantial discrepancy between the two tested replicates or for which one or two of the measurements had been disrupted due to technical errors.

The 214 compounds (104 + 110) identified in the primary screen were subjected to a secondary screen (**Fig. 4a**). This was done in a similar manner except that a smaller device was used, the spotted compound concentration was tenfold lower than in the primary screen and five replicates were spotted for each compound. Eighteen compounds were confirmed to substantially inhibit RNA binding by NS4B out of the 214 compounds tested (**Fig. 4b**). Six of these compounds were tested for specificity; five of them did not inhibit binding of HuR protein to its own 4A target RNA sequence (**Supplementary Fig. 3**) nor did they inhibit HuR binding to its previously described HCV RNA target, that is the 3′ terminus of the negative viral strand[27], suggesting that these hits are specific. This data and additional data supporting the validity of the screen are presented in **Supplementary Data** and **Supplementary Fig. 5** online.

Inhibitors of HCV RNA replication

We measured the inhibitory effect on HCV RNA replication of the compounds identified in the above screen in cell culture. After electroporation with a full-length HCV RNA genome harboring a luciferase reporter gene[28], Huh7.5 cells were grown in the presence of increasing concentrations of these compounds. Luciferase assays were performed at 72 h. In parallel, the viability of cells in the presence of the compounds was assessed by an Alamar Blue–based assay. Six of the compounds showed some antiviral effect above that solely attributable to cellular toxicity. One of these, clemizole hydrochloride (1-*p*-chlorobenzyl-2-(1-pyrrolidinyl) methylbenzimidazole hydrochloride), an H1 histamine receptor antagonist, was found to substantially inhibit HCV replication. A tenfold decrease in viral replication was measured at 20 μM concentration of the drug, with an half-maximal effective concentration (EC_{50}) of ~8 μM (**Fig. 4c**). At these concentrations there was no measurable cellular toxicity (**Fig. 4c**). Similar results were obtained by real-time PCR assays performed in clemizole-treated Huh7.5 cells infected with the infectious HCV clone (J6/JFH)[29] (**Supplementary Fig. 6** online). The *in vitro* half-maximal inhibitory concentration (IC_{50}) of clemizole for RNA binding by NS4B is ~24 ± 1 nM (**Fig. 4d**).

Clemizole-resistant mutants

The mechanism of action of clemizole's antiviral activity was further substantiated by selecting for clemizole-resistant HCV mutants. Established HCV replicon-harboring cells and Huh7 cells electroporated *de novo* with a genotype 1b subgenomic HCV replicon (Bart 79I)[30] were passaged in the presence of the drug, yielding

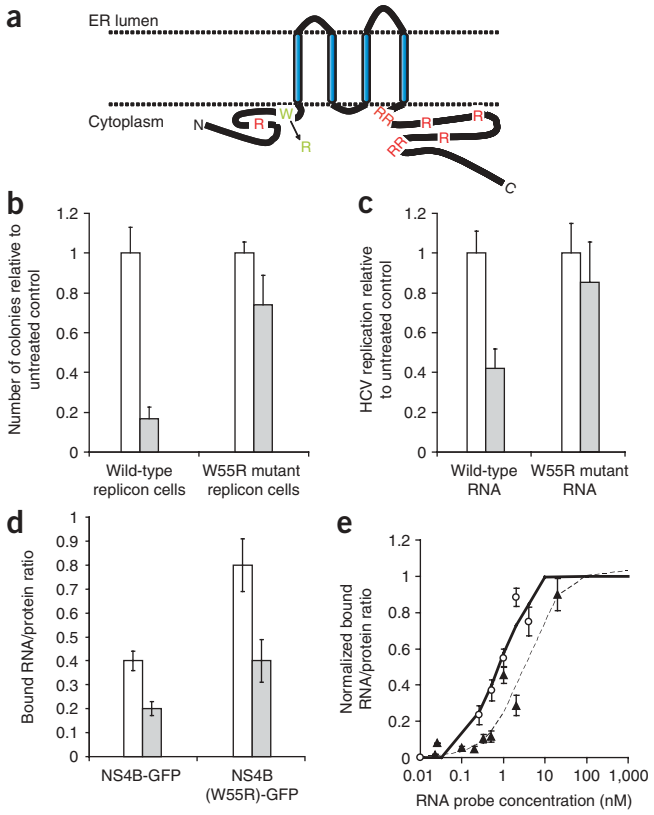

Figure 5 Clemizol-resistant mutant. Replicon cells were passaged in the presence of clemizole and individual colonies were isolated, propagated and the HCV genomes harbored within were subjected to sequence analysis. (**a**) Schematic diagram indicating predicted transmembrane and intracellular segments of NS4B. Conserved positively charged amino acids are shown in red. The clemizole-resistant mutation, W55R, is shown in green. (**b**) HCV replication in Huh7.5 cells electroporated with 50 μg of whole-cell RNA extracted from cells harboring either wild type or the W55R mutant clone, followed by growth in the absence (white bars) or presence (gray bars) of 10 μM clemizole. Results represent relative numbers of colonies obtained compared to each corresponding untreated control. (**c**) HCV replication assays initiated by electroporation of *in vitro* transcribed luciferase reporter–linked wild-type or W55R mutant HCV RNA genomes performed in the absence (white bars) or presence (gray bars) of 10 μM clemizole. Results represent replication level of each genome relative to its untreated level. (**d**) HCV RNA binding of wild-type NS4B and the W55R NS4B mutant as measured *in vitro* by microfluidics in the presence of 10 nM clemizole (gray bars) and its absence (white bars). (**e**) *In vitro* binding curves of W55R NS4B mutant (solid line, ○) and wild-type NS4B (broken line, ▲) to serial dilutions of the RNA probe. Each data point represents the mean of 10–20 replicates, and the bars represent the standard error.

~60 colonies that were able to grow in the presence of the compound. Eleven individual colonies were successfully expanded, passaged 5–10 times and the HCV RNA replicating in the cells was subjected to sequence analysis. In addition, RNA from a pool of clemizole-resistant colonies was isolated and subjected to a similar analysis. Three colonies were found to harbor replicons with mutations that mapped to the NS4B region, and six colonies were found to harbor replicons with mutations that mapped to the negative strand 3′ terminus RNA region. In addition there was one colony with mutations that mapped to both NS4B and the negative strand 3′ terminus, and one where we have yet to find the location of the mutation conferring resistance to clemizole. No such mutations were identified in ten replicon colonies that were passaged in parallel in the absence of the drug.

Two of the clemizole-resistant NS4B mutants were characterized in detail. The first, W55R is depicted in **Figure 5a**. It involves the substitution of an arginine for the tryptophan at amino acid 55 within a predicted cytoplasmically oriented segment of NS4B. This mutation is sufficient to confer a clemizole-resistant phenotype in cells: Huh7.5 cells transfected with either whole-cell RNA extracted from the W55R mutant cells (**Fig. 5b**) or with *in vitro*-transcribed J6/JFH RNA encoding this point mutation and a linked luciferase reporter gene (**Fig. 5c**) were unaffected by 10 μM clemizole. The EC_{50} of clemizole on the W55R mutant J6/JFH RNA was ~18 μM (2.25 times the EC_{50} of the wild-type RNA). Similar to other HCV mutants resistant to an NS3 protease inhibitor[31], the absolute level of replication of the W55R mutant was lower than that of the wild-type genome, suggesting that the drug-resistant mutation comes at the cost of impaired replication fitness.

We also introduced this mutation into the NS4B-GFP vector and tested it for its RNA binding activity using the *in vitro* microfluidic assay. Although both mutant and wild-type NS4B proteins experienced an approximately twofold reduction of RNA binding in the presence of 10 nM clemizole, because the baseline RNA binding of the mutant is higher, the residual amount of RNA bound by the mutant in the presence of clemizole was comparable to that bound by the wild type in the absence of clemizole (**Fig. 5d**). Furthermore, this mutant demonstrates greater apparent affinity to the viral RNA with a K_d of 0.75 nM (versus 3.4 nM for wild-type NS4B) (**Fig. 5e**).

The second clemizole-resistant mutation, termed R214Q, was identified in a resistant colony as well as in pooled resistant cells. It involves the substitution of a glutamine for the arginine at amino acid 214 within the cytoplasmic C-terminal segment of NS4B. Similar results to the first mutation were obtained in cellular and *in vitro* analyses done on this mutation, with an EC_{50} of 40.3 μM (~5 times higher than the EC_{50} on the wild-type RNA) in the luciferase reporter–linked replication assay and a K_d of 0.6 nM in the *in vitro* binding assay (data not shown). Presumably both of these mutations alter the conformation of NS4B so as to increase its affinity for the viral RNA. Indeed the K_ds measured by the *in vitro* RNA binding assay reflect this. Taken together, the above data provide genetic and biochemical evidence for clemizole's mechanism of action.

DISCUSSION

The above results demonstrate that HCV NS4B binds RNA and that this binding is specific for the 3′ terminus of the negative strand of the viral genome. Because the *in vivo* specificity of this interaction has not yet been determined quantitatively, one should use the usual caution in extrapolating the numerical value of our *in vitro* results. We also showed that an arginine rich–like motif in NS4B is essential for RNA binding and for HCV replication. Clemizole hydrochloride was found to have a substantial inhibitory effect on HCV RNA replication mediated by its suppression of NS4B's RNA binding.

Because NS4B is associated with membranes[5] and is known to induce membrane replication sites[4], its RNA binding activity offers a mechanism to incorporate the viral genome into the HCV replication compartment. This may facilitate the initiation of synthesis of the nascent positive strand from the membrane-anchored negative strand. NS4B may also act by recruiting the polymerase complex to the HCV RNA, through its interaction with the NS5B polymerase or other components of the replication complex[32].

The *in vitro* IC_{50} of clemizole for RNA binding by NS4B is ~24 ± 1 nM, whereas its EC_{50} for viral replication is ~8 μM. It is possible that poor cellular permeability accounts for the ~400-fold difference between the IC_{50} measured for *in vitro* RNA binding by NS4B and the EC_{50} measured for the antiviral effect in cells. We hypothesize that improved drug delivery and optimization of the compound after structure-activity relationship analysis will improve its potency as an antiviral agent and that the microfluidic platform can facilitate this process.

This study also demonstrates the utility of a microfluidic approach. The microfluidic affinity assay has several important advantages over currently used methods, which make it a promising and general tool for drug discovery, especially against membrane-bound targets. First, protein synthesis by mammalian reticulocyte lysates in the presence of microsomal membranes provides the natural conditions required for protein folding. Second, the microfluidic assay eliminates the need for a high level of protein expression and purification, a problem common to currently used methods. Third, this assay is capable of detecting transient and low-affinity interactions[15]. Fourth, the microfluidic device is capable of making many parallel measurements, and therefore can be used for high-throughput screening. Finally, we have shown, in spite of known chemical compatibility issues with the elastomer used to fabricate the device, that one can successfully screen and discover small molecules with desired pharmacological properties.

As with HIV and tuberculosis, effective pharmacologic control of HCV will likely best be achieved by a cocktail of several drugs against independent virus-specific targets. Combination of even a moderate NS4B inhibitor with other emerging anti-HCV agents represents an attractive paradigm for increasing current virologic response rates. Although we hypothesize that more potent inhibitors than clemizole can be obtained, because clemizole has already been extensively used in humans (albeit for a different indication based on its antipruritic properties) it may find immediate use as a critical component of next generation anti-HCV strategies.

METHODS

Plasmids. Standard recombinant DNA technology was used to construct and purify all plasmids. All regions that were amplified by PCR were analyzed by automated DNA sequencing. Plasmid DNAs were prepared from large-scale bacterial cultures and purified by aMaxiprep kit (Marligen Biosciences). Restriction enzymes were purchased from New England Biolabs.

The open reading frames (ORF) of HuR and HuD were obtained from the ORFeome library of cDNA clones (Open Biosystems). These ORFs were inserted into the expression vectorpcDNA-Dest 40 vector (Invitrogen) by the use of gateway technology (Invitrogen) allowing addition of a C-terminal V5-his tag.

The plasmid pcDNA-NS4B-GFP encoding NS4B of genotype 1a fused in frame with a C-terminal GFP was previously described[5]. The mutations RRa, RRb and W55R were introduced into this plasmid by site-directed mutagenesis (using the QuikChange kit (Stratagene)). The plasmid NS5A(AH)GFP was constructed as previously reported. Gus-his vector was obtained from Roche.

The plasmids pcDNA3.1-5′ UTR pos, which encodes the 5′ UTR of the positive viral strand, was generated by amplification of the 5′ UTR positive sequence from the Bart79I plasmid[33] with primers containing *Eco*RV restriction sites, digestion with *Eco*RV and ligation into the corresponding site in pcDNA3.1 (Invitrogen). The plasmid pcDNA3.1- 3′ negative terminus, which encodes the 3′ terminal region of the negative RNA strand, was generated the same way except that the *Eco*RV-flanked insert was ligated in an inverse orientation.

The plasmids pcDNA3.1 – 3′ UTR pos and 5′ negative terminus were similarly generated except that the inserted gene was flanked by *Hin*dIII and *Xho*1 restriction sites.

The vector encoding the delta virus genomic RNA sequence was cloned by inserting *Nhe*I-flanked HDV sequence into a pSPT19 vector (Roche Diagnostics) cut with *Xba*I[23,24].

The plasmid FL-J6/JFH-5′C19Rluc2AUbi that consists of the full-length HCV genome and expresses *Renilla* luciferase was a gift from Charles M. Rice[28]. The W55R mutation was introduced into this plasmid by site-directed mutagenesis (using the QuikChange kit).

***In vitro* RNA transcription and fluorescent and radioactive labeling.** Plasmid DNA of the 5′ and 3′ terminal regions of the negative and positive viral strands were linearized with *Xba*I. The plasmid DNA of the delta genomic sequence was linearized with *Xba*I. Linearized plasmids were then treated with proteinase K, followed by phenol-chloroform extraction and precipitation with ethanol. The DNA was resuspended in RNase-free water to a final concentration of 1 μg/μl. We used 4 μg of DNA as a template for transcription with the T7 MEGAscript (Ambion) according to the manufacturer's protocol. The template DNA was digested by the addition of 5 U of RQ1 DNase (Ambion) and a 15-min incubation at 37 °C. The unincorporated ribonucleotides were removed by size exclusion with a Micro Bio-Spin P-30 column (Bio-Rad), and the transcribed RNA was extracted with phenol-chloroform, followed by precipitation in ethanol. The RNA pellet was washed with 70% ethanol and resuspended in H_2O. Determination of the RNA concentration was performed by measurement of the optical density at 260 nm. The integrity of the RNA and its concentration were confirmed by 1% agarose gel electrophoresis and ethidium bromide staining.

The RNA sequences were labeled with Cy5 by using Label IT kit (Mirus) according to the manufacturer's protocol followed by purification on a microspin column (Mirus) and ethanol precipitation. The number of fluorescent labels per RNA molecule was determined by measuring the spectrophotometric absorbance of the nucleic-dye conjugate at 260 nm and the λ_{MAX} for Cy5 (650 nm). This was proportional to the probe's length and was used to adjust our binding experiments results.

Cy3-labeled RNA probes used to study RNA binding by HuR and HuD were purchased from IDT.

Radioactive labeling of RNA probes with ^{32}P was done as previously described[34].

Device design. Device fabrication and design was done essentially as described[15]. In brief, a 'control' layer, which harbors all channels required to actuate the valves, is situated on top of a 'flow' layer, which contains the network of channels being controlled. All biological assays and fluid manipulations are performed on the flow layer. A valve is created where a control channel crosses a flow channel. The resulting thin membrane in the junction between the two channels can be deflected by hydraulic actuation. Using multiplexed valve systems allows a large number of elastomeric microvalves to perform complex fluidic manipulations within these devices. Introduction of fluid into these devices is accomplished through stainless steel pins inserted into holes punched through the silicone. Computer-controlled external solenoid valves allow actuation of multiplexors, which in turn allow complex addressing of a large number of microvalves. Each unit cell is controlled by three micromechanical valves as well as a 'button' membrane (**Supplementary Fig. 1**). The 'button membrane' of each unit cell masks a circular area within the flow channel between two 'sandwich' valves. Aligning and bonding a microarray to the device allows positioning of the spotted material (RNA probes or inhibitory compounds) within the 'RNA chamber' of each unit cell. This chamber can then be opened to the flow channel by the control of a 'neck valve'. Devices had either 640 or 2,400 unit cells.

RNA binding assay. The approach used was a modification of the previously described method for protein-DNA interactions[15] (**Supplementary Fig. 1**).

For soluble proteins: RNA arraying and device alignment. A dilution series of Cy3-labeled target RNA sequences were spotted as a microarray onto epoxy-coated glass substrates slide (CEL Associates) by OmniGrid Micro (GeneMachines) microarrayer using a CMP3B pin (TeleChem International) with column and row pitches of 680 mm and 320 mm, respectively. Each sample solution contained 1% BSA in dH_2O to prevent covalent linkage of the target RNA to the epoxy functional groups as well as for visualization during

alignment. After spotting the arrays were quality controlled on a GenePix4000b (Molecular Devices). The arrays were then aligned to a microfluidic device by hand on a SMZ1500 (Nikon) stereoscope and bonded overnight in the dark on a heated plate at 40 °C.

Surface chemistry (**Supplementary Fig. 1c** *online*). All devices were driven between 10 and 15 p.s.i. in the control line and between 4 and 6 p.s.i. for the flow line. For the initial surface-derivatization steps the chamber valves remained closed to prevent liquid from entering the chambers containing the spotted RNA targets. First, all accessible surface area was derivatized by flowing a solution of biotinylated BSA (Pierce) resuspended to 2 mg/ml in dH_2O for 30 min through all channels, followed by a 10 min PBS wash. Next a 500 μg/ml neutravidin (Pierce) solution in PBS was flowed for 20 min, followed by a 10 min PBS wash. Next, the button membrane was closed and the PBS wash continued for an additional 5 min. Then all remaining accessible surface area except for the circular area of 60 μm masked by the button was passivated with the same biotinylated solution as above for 30 min, followed by a 10 min PBS wash. Finally a 1:1 solution ofbiotinylated-5-histidine antibody (Qiagen) in 2% BSA in PBS was loaded for 2–5 min, after which the button membrane was opened and flow continued for 20 min allowing specific functionalization of the previously masked circular area. This was again followed by a 10 min PBS wash completing the surface derivatization procedure.

Protein synthesis and MITOMI. Next a standard 25 μl TNT T7–coupled wheat germ extract mixture (Promega) was prepared and spiked with 1 μl tRNA*Lys-bodipy-fl* (Promega) and 2 μl of plasmid DNA template coding for the appropriate protein (HuR, HuD or Gus). The mixture was immediately loaded into the device and flushed for 5 min, after which the chamber valves were opened allowing for dead-end filling of the chambers with wheat germ extract. The chamber valves were again closed and flushing continued for an additional 5 min. Next the segregation valves separating each unit cell were closed followed by opening of the chamber valves allowing for equilibration of the unit cell by diffusion. The entire device was heated to 30 °C on a temperature-controlled microscope stage and incubated for up to 90 min to complete protein synthesis, binding of protein to the surface-bound biotinylated-5-histidine antibody, solvation of target RNA, and equilibration of proteins and target RNA. MITOMI was then performed by closing the button membrane as well as the chamber valves allowing trapping surface-bound complexes while expelling any solution phase molecules. Radial closure prevents solvent pockets from forming between the two interfaces and effectively creates zero dead volume while preserving the equilibrium concentrations of the molecular interactions. This was followed by a 5 min PBS wash to remove untrapped unbound material. The device was then imaged on a modified arrayWoRx*e* (AppliedPrecision) microarray scanner to detect protein synthesis and the trapped molecules.

Image and data analysis. All images were analyzed with GenePix3.0 (Molecular Devices). For each experiment an image was taken after MITOMI and the final PBS wash. This was used to determine the concentration of surface-bound protein (FITC channel) as well as surface-bound target RNA (Cy3 channel). Each unit cell generated a single data point that consisted of the ratio of median signal of Cy3 to median signal of bodipy; thus, representing the ratio of surface-bound RNA to surface-bound expressed protein. Data from multiple data points were averaged and their s.d. calculated. Results were then normalized to 1. Between 10 and 20 replicates were included for each probe tested. A control protein, Gus-his (Roche) was included in each experiment and subjected to the same analysis. When present, detected signal with Gus-his was used for background subtraction.

For membrane-associated proteins. Detection of RNA binding by NS4B was done as described except for the following modifications. NS4B was expressed off the microfluidic device by using a coupled transcription/translation rabbit reticulocyte system (Promega). We added 2 μl canine microsomal membranes (Promega) to the reaction mixture to allow appropriate protein folding. An NS4B-GFP construct was used thus eliminating the need for tRNA*Lys–bodipy–fl* in the reaction mixture. A biotinylated anti-GFP antibody (Abcam) was used to specifically functionalize the protected circular area defined by the button. The protein was anchored to the chip via its interaction with the surface-bound anti-GFP antibodies. The surface-bound protein and the Cy5-labeled HCV RNA probes were loaded into the chip and allowed to incubate for 5–20 min in a 50-mM HEPES KOH (pH 6.8) buffer. Next, MITOMI was performed followed by a brief wash in HEPES KOH (pH 6.8) buffer. The device was then scanned and results quantified as described above. NS4B-GFP mutants and NS5A(AH)-GFP were assayed the same way. Signal detected with NS5A(AH)-GFP was used for background subtraction.

Screening of inhibitory compound library. The 1,280 compounds of the Lopac library (Sigma) solubilized in DMSO were spotted onto epoxy-coated glass substrates slide by OmniGrid Micro microarrayer using a CMP3B pin as a microarray. For the primary screen compounds were spotted at a high concentration (~1 mM) in duplicates. The array was allowed to dry and was then aligned and bonded to a microfluidic device. Two large devices (2,400 unit cells per device) were used for the primary screen. The rest of the procedure was done similarly to the described above (RNA binding assay). In brief, the device was subjected to surface patterning that resulted in a circular area coated with biotinylated anti-GFP antibodies within each unit cell. Next, NS4B-GFP expressed off chip using coupled transcription/translation rabbit reticulocyte system in the presence of microsomal membranes was loaded into the chip and bound to the surface biotinylated anti-GFP antibodies. Cy5-labeled 3′ neg terminus RNA probe was then loaded at a concentration of 1.5 nM. Each unit cell was then isolated followed by a 30 min incubation to allow binding of the protein to surface-biotinylated anti-GFP antibodies, solvation of library compounds, and equilibration of proteins and target RNA. Next, MITOMI was performed trapping surface-bound complexes while expelling any solution phase molecules. After a brief wash to remove untrapped unbound material the device was scanned and results analyzed. The ratio of bound RNA to expressed protein was calculated for each data point by measuring the median signal of Cy3 to median signal of bodipy. Results were normalized to signal measured in unit cells containing no inhibitory compound. Greater than 90% inhibition was defined as the cutoff for inhibition in the primary screen; 104 compounds which were above this cutoff and an additional 110 yielding ambiguous results were subjected to a secondary screen. This was performed similarly, except that two smaller devices (640 unit cells per each) were used; the spotted compound concentration was 10-fold lower than in the primary screen, and five replicates were spotted for each compound. Inhibition >2.5 fold was considered significant. 18 compounds identified in this screen were further analyzed for their inhibitory effect on HCV RNA replication.

Determination of IC_{50} for *in vitro* RNA binding. For an accurate measurement of IC_{50}s, serial dilutions of the inhibitory compound were loaded onto the microfluidic device by continuous flow while maintaining a steady concentration of the compound in the flow channel. This helped to avoid losses of the spotted compounds from incomplete solubilization and/or binding of the compound to PDMS. The experiment was performed essentially as described in the RNA binding assay for transmembrane proteins except that the expressed protein and the Cy5-labeled HCV RNA probes were incubated in the device in the presence of the inhibitory compounds or their absence. IC_{50}s were measured as described in the statistical analysis section below.

Expression and purification of recombinant NS4B. GST-NS4B and GST were expressed in *E. coli* BL21 and purified as described elsewhere[11]. NS4B was fused in frame with an N-terminal 6his-MISTIC protein (membrane-integrating sequence for translation of IM protein constructs)[35]. Overnight cultures of *E. coli* transformed with mistic-NS4B plasmid were diluted 1:100 in 400 ml of fresh medium and grown at 37 °C to an OD of 0.8. IPTG (Invitrogen) was then added to a final concentration of 0.1 mM. After 3 h growth at 37 °C cells were pelleted and resuspended in 30cml lysis buffer (50 mM NaCl, 50 mM Tris HCL (pH8), 100 mM imidazole, 10 mM decylmaltoside, Complete EDTA-free protease inhibitors (Roche Applied Science)). Cells were lysed by one cycle in a French Press at a pressure of 10,000 p.s.i. for 1 min, followed by centrifugation at 12,000*g* for 5 min at 4 °C. The supernatant was loaded on a nickel column (Amersham). After washes, protein was eluted in a buffer containing 400 mM imidazole. Glycerol was added at a final concentration of 20% and samples were stored at –20 °C. Purification was monitored by SDS-PAGE. Total protein concentration was measured using the RC-DC assay (Bio-Rad). NS4B-mistic was identified by western blot analyses using monoclonal antibodies against

6-his (Santa Cruz Biotechnology) and NS4B (Virostat). 6his-mistic was expressed and purified in a similar manner.

GST pull-down assay. Similar to a previously described strategy[36], 1 μg of purified GST-NS4B or GST was incubated for 1 h at 37 °C in a 50 μl reaction mixture containing ^{32}P-labeled *in vitro*–transcribed HCV RNA (corresponding to the 3′ terminus of the negative viral strand) and binding buffer (10 mM DTT, 10 mM Na HEPES (pH 7.4), 33 mM NaCl, 0.1 mM EDTA, 10 mM MgCl2). We then added 50 μl oftRNA precoated glutathione-agarose beads (Sigma), followed by 1 h incubation at 4 °C to allow binding of GST to the beads. The beads were then washed three times in binding buffer and bound RNA was measured by liquid scintillation counting of sample aliquots. Control incubations with an RNA probe prepared in the absence of T7 RNA polymerase were used for background subtraction.

RNA filter binding assay. Assays were performed essentially as described[34]. Briefly, various concentrations of mistic-NS4B protein or mistic control were incubated for 1 h at 30 °C with 3.3 nM ^{32}P-labeled *in vitro*–transcribed HCV RNA probe in binding buffer (50 mM HEPES pH 7.0, 50 mM NaCl, 1 mM MgCl2, 10 ng/μl tRNA and 0.2 mM decylmaltoside) in a final volume of 40 μl. Membranes were presoaked in the binding buffer and assembled in a dot-blot apparatus (Schleicher & Schull) from top to bottom as follows: nitrocellulose (Biorad), Hybond N+ (Amersham Biosciences), Whatman 3-mm filter paper. The binding reactions were loaded onto the dot-blot apparatus and filtered through the membranes. After washing, the membranes were air-dried and visualized by phospho-imaging. Results represent percentage of bound RNA calculated by dividing the signal detected in the nitrocellulose membrane by the sum of the signals detected in the nitrocellulose and the Hybond membranes.

Cell culture and electroporation. Huh7.5 cells were maintained in DMEM (Gibco) supplemented with 1% L-glutamine (Gibco), 1% penicillin, 1% streptomycin (Gibco), 1× nonessential amino acids (Gibco) and 10% FBS (Omega Scientific). Cell lines were passaged twice weekly after treatment with 0.05% trypsin–0.02% EDTA and seeding at a dilution of 1:5. Subconfluent Huh7.5 cells were trypsinized and collected by centrifugation at 700*g* for 5 min. The cells were then washed three times in ice-cold RNase-free PBS (BioWhittaker) and resuspended at 1.5×10^7 cells/ml in PBS. Wild-type or mutant FL-J6/JFH-5′C19Rluc2AUbi RNA for electroporation was generated by *in vitro* transcription of *Xba*I-linearized DNA templates using the T7 MEGAscript kit (Ambion), followed by purification, essentially as described above (*in vitro* RNA transcription and fluorescent labeling). We mixed 5 μg of RNA with 400 μl of washed Huh7.5 cells in a 2-mm-gap cuvette (BTX) and immediately pulsed (0.82 kV, five 99 μs pulses) with a BTX-830 electroporator. After a 10 min recovery at 25 °C, pulsed cells were diluted into 10 ml of prewarmed growth medium. Cells from several electroporations were pooled to a common stock and seeded in 6-well plates (5×10^5 cells per well). After 24 h, medium was replaced and cells were grown in the presence of serial dilutions of the various inhibitory compounds (Sigma) identified in the screen. Seventeen commercially available compounds, out of the 18 identified, were analyzed. Untreated cells were used as a negative control for water-soluble compounds. For compounds solubilized in DMSO, untreated cells were grown in the presence of corresponding concentrations of the solvent as a negative control. Medium was changed daily. After 72 h of treatment cells were subjected to an Alamar Blue–based viability assay and luciferase assay.

Viability assay. After 72 h of treatment cells were incubated for 3 h at 37 °C in the presence of 10% Alamar Blue reagent (TREK Diagnostic Systems). Plates were then scanned and fluorescence was detected by using FLEXstation II 384 (Molecular Devices). Depending on the inhibitory compound's solvent, water or DMSO, signal was normalized relatively to untreated samples or samples grown in the presence of DMSO, respectively.

Luciferase assay. Viral RNA replication was determined using *Renilla* luciferase assay (Promega). The same samples subjected to the viability assay described above were analyzed in this assay. Cells were washed with ice-cold PBS and scraped off the plate into 250 μl of ice-cold *Renilla* lysis buffer according to the manufacturer's protocol. We then loaded 20 μl of the cell lysates onto 96-well plates. We injected 100 μl of the *Renilla* luciferase assay buffer containing the assay substrate and measured luciferase activity using a Berthold LB 96 V luminometer. As above, signal was normalized relative to untreated samples or samples grown in the presence of the corresponding concentration of DMSO.

Luciferase activity detected in samples treated with 100 u/ml interferon α B2 (PBL Biomedical Labs) was used as a positive control, demonstrating three log reduction at 72 h treatment. The experiment was repeated four times, each time with triplicates. IC_{50}s were measured by fitting data to a three-parameter logistic curve using the formula Y = a+(b – a)/(1 + 10^(X – c)) (BioDataFit, Chang Bioscience).

Real-time PCR. 5×10^4 Huh7.5 ells were infected with cell culture-grown HCV titered at 1.4×10^4 $TCID_{50}$/ml, as described[29]. Two hours after infection, cells were washed three times in culture medium. Cells were then treated daily with various concentrations of clemizole. After 72 h samples were subjected to the viability assay described above, following which TRIzol Reagent (Invitrogen) was added and total cell RNA was extracted in triplicates according to the manufacturer's instructions. Reverse transcription was then performed using random hexamers and Superscript II reverse transcriptase (Invitrogen). Real-time PCR was performed on the resulting cDNA to quantify the amounts of HCV and actin RNA (in separate reactions) in each sample. Standards were made using an *in vitro*-transcribed HCV RNA and human actin standard (Applied Biosystems). HCV was quantified using primers AGAGCCATAG TGGTCT and CCAAATCTCCAGGCATTGAGC and probe 6-carboxyfluorescein-CACCGGAATTGCCAGGACGACCGG-6-carboxytetramethylrhodamine. Actin was quantified using beta-actin control reagents (Applied Biosystems) according to the manufacturer's instructions. HCV RNA level was adjusted to actin level and normalized relative to untreated samples.

Selection of resistant mutants. Established HCV replicon-harboring cells and Huh7 cells electroporated *de novo* with a genotype 1b subgenomic HCV replicon (Bart 79I)[30] were passaged in the presence of neomycin and increasing concentration of clemizole (1-16 μM). Colonies that were able to grow in the presence of the compound were isolated and propagated for 5–10 passages. Eleven colonies (out of ~60) survived the passages and were subjected to sequence analysis, as previously described[11].

Whole-cell RNA electroporation. Whole-cell RNA was extracted from clemizole-resistant replicon clones and from untreated replicon cells using TRIzol reagent. Equal amounts of whole cell RNA (50 μg) were electroporated into Huh7.5 cells, as described above. Cells were grown under G418 selection in the presence or absence of clemizole for 3 weeks. The number of colonies was determined using Image J (National Institutes of Health) following fixation and staining with crystal violet.

Statistical analysis. Dissociation equilibrium constants were determined by fitting data to the equation describing equilibrium binding; Y = a × X/(b + X) (a and b represent maximum binding and K_d, respectively) by nonlinear least-squares regression fitting (BioDataFit, Chang Bioscience). IC_{50}s were measured by fitting data to a three-parameter logistic curve using the formula Y = a + (b – a)/(1 + 10^(X – c)) (a, b and c represent minimum binding, maximum binding and logEC_{50}, respectively)(BioDataFit, Chang Bioscience).

Note: Supplementary information is available on the Nature Biotechnology website.

ACKNOWLEDGMENTS

This work was supported by a Burroughs Wellcome Fund Clinical Scientist Award in Translational Research (to J.S.G.) and National Institutes of Health (NIH) RO1 DK066793, an NIH Director's Pioneer Award (to S.R.Q.) and NIH 1RO1 HG002644-01A1. D.G. was supported in part by the Fulbright Foundation. S.E. is a recipient of an American Liver Foundation Postdoctoral Fellowship Award. We also wish to thank the Stanford University SPARK Program, High-Throughput Bioscience Center and the Microfluidic Foundry. The plasmid FL-J6/JFH-5′C19Rluc2AUbi that consists of the full-length HCV genome and expresses *Renilla* luciferase was a gift from Charles M. Rice, Rockefeller University.

COMPETING INTERESTS STATEMENT

The authors declare competing financial interests: details accompany the full-text HTML version of the paper at http://www.nature.com/naturebiotechnology/

Published online at http://www.nature.com/naturebiotechnology/
Reprints and permissions information is available online at http://npg.nature.com/reprintsandpermissions/

1. Liang, T.J., Rehermann, B., Seeff, L.B. & Hoofnagle, J.H. Pathogenesis, natural history, treatment, and prevention of hepatitis C. *Ann. Intern. Med.* **132**, 296–305 (2000).
2. Reed, K.E. & Rice, C.M. Overview of hepatitis C virus genome structure, polyprotein processing, and protein properties. *Curr. Top. Microbiol. Immunol.* **242**, 55–84 (2000).
3. Rice, C.M. Flaviviridae: The viruses and their replication. in *Fields Virology* (eds. Fields, B.N., Knipe, D.M. & Howley, P.M.) 991–1041 (Lippincott-Raven Publications, Philadelphia, 1996).
4. Egger, D. *et al.* Expression of hepatitis C virus proteins induces distinct membrane alterations including a candidate viral replication complex. *J. Virol.* **76**, 5974–5984 (2002).
5. Elazar, M., Liu, P., Rice, C.M. & Glenn, J.S. An N-terminal amphipathic helix in hepatitis C virus (HCV) NS4B mediates membrane association, correct localization of replication complex proteins, and HCV RNA replication. *J. Virol.* **78**, 11393–11400 (2004).
6. Gosert, R. *et al.* Identification of the hepatitis C virus RNA replication complex in Huh-7 cells harboring subgenomic replicons. *J. Virol.* **77**, 5487–5492 (2003).
7. El-Hage, N. & Luo, G. Replication of hepatitis C virus RNA occurs in a membrane-bound replication complex containing nonstructural viral proteins and RNA. *J. Gen. Virol.* **84**, 2761–2769 (2003).
8. Kusov, Y.Y., Probst, C., Jecht, M., Jost, P.D. & Gauss-Müller, V. Membrane association and RNA binding of recombinant hepatitis A virus protein 2C. *Arch. Virol.* **143**, 931–944 (1998).
9. Rodríguez, P.L. & Carrasco, L. Poliovirus protein 2C contains two regions involved in RNA binding activity. *J. Biol. Chem.* **270**, 10105–10112 (1995).
10. Echeverri, A.C. & Dasgupta, A. Amino terminal regions of poliovirus 2C protein mediate membrane binding. *Virology* **208**, 540–553 (1995).
11. Einav, S., Elazar, M., Danieli, T. & Glenn, J.S. A nucleotide binding motif in hepatitis C virus (HCV) NS4B mediates HCV RNA replication. *J. Virol.* **78**, 11288–11295 (2004).
12. Overington, J.P. Al-Lazikani, B. & Hopkins AL. How many drug targets are there? *Nat. Rev. Drug Discov.* **5**, 993–996 (2006).
13. Lundin, M., Monné, M., Widell, A., Von Heijne, G. & Persson, M.A.A. Topology of the membrane-associated hepatitis C virus protein NS4B. *J. Virol.* **77**, 5428–5438 (2003).
14. Hadd, A.G., Raymond, D.E., Halliwell, J.W., Jacobson, S.C. & Ramsey, J.M. Microchip device for performing enzyme assays. *Anal. Chem.* **69**, 3407–3412 (1997).
15. Maerkl, S.J. & Quake, S.R. A systems approach to measuring the binding energy landscapes of transcription factors. *Science* **315**, 233–237 (2007).
16. Toepke, M.W. & Beebe, D.J. PDMS absorption of small molecules and consequences in microfluidic applications. *Lab Chip* **6**, 1484–1486 (2006).
17. Lee, J.N., Park, C. & Whitesides, G.M. Solvent compatibility of poly(dimethylsiloxane)-based microfluidic devices. *Anal. Chem.* **75**, 6544–6554 (2003).
18. Whitesides, G.M. The origins and the future of microfluidics. *Nature* **442**, 368–373 (2006).
19. Kang, L., Chung, B.G., Langer, R. & Khademhosseini, A. Microfluidics for drug discovery and development: from target selection to product lifecycle management. *Drug Discov. Today* **13**, 1–13 (2008).
20. Myer, V.E., Fan, X.C. & Steitz, J.A. Identification of HuR as a protein implicated in AUUUA-mediated mRNA decay. *EMBO J.* **16**, 2130–2139 (1997).
21. Park, S., Myszka, D.G., Yu, M., Littler, S.J. & Laird-Offringa, I.A. HuD RNA recognition motifs play distinct roles in the formation of a stable complex with AU-rich RNA. *Mol. Cell. Biol.* **20**, 4765–4772 (2000).
22. Park-Lee, S., Kim, S. & Laird-Offringa, I.A. Characterization of the interaction between neuronal RNA-binding protein HuD and AU-rich RNA. *J. Biol. Chem.* **278**, 39801–39808 (2003).
23. Glenn, J.S., Taylor, J.M. & White, J.M. In vitro-synthesized hepatitis delta virus RNA initiates genome replication in cultured cells. *J. Virol.* **64**, 3104–3107 (1990).
24. Glenn, J.S., Watson, J.A., Havel, C.M. & White, J.M. Identification of a prenylation site in delta virus large antigen. *Science* **256**, 1331–1333 (1992).
25. Burd, C.G. & Dreyfuss, G. Conserved structures and diversity of functions of RNA-binding proteins. *Science* **265**, 615–621 (1994).
26. Wung, C.H. *et al.* Identification of the RNA-binding sites of the triple gene block protein 1 of bamboo mosaic potexvirus. *J. Gen. Virol.* **80**, 1119–1126 (1999).
27. Spångberg, K., Wiklund, L. & Schwartz, S. HuR, a protein implicated in oncogene and growth factor mRNA decay, binds to the 3′ ends of hepatitis C virus RNA of both polarities. *Virology* **274**, 378–390 (2000).
28. Tscherne, D.M. *et al.* Time- and temperature-dependent activation of hepatitis C virus for low-pH-triggered entry. *J. Virol.* **80**, 1734–1741 (2006).
29. Lindenbach, B.D. *et al.* Complete replication of hepatitis C virus in cell culture. *Science* **309**, 623–626 (2005).
30. Elazar, M. *et al.* Amphipathic helix-dependent localization of NS5A mediates hepatitis C virus RNA replication. *J. Virol.* **77**, 6055–6061 (2003).
31. Tong, X. *et al.* Identification and analysis of fitness of resistance mutations against the HCV protease inhibitor SCH 503034. *Antiviral Res.* **70**, 28–38 (2006).
32. Dimitrova, M., Imbert, I., Kieny, M.P. & Schuster, C. Protein-protein interactions between hepatitis C virus nonstructural proteins. *J. Virol.* **77**, 5401–5414 (2003).
33. Blight, K.J., Kolykhalov, A.A. & Rice, C.M. Efficient initiation of HCV RNA replication in cell culture. *Science* **290**, 1972–1974 (2000).
34. Huang, L. *et al.* Hepatitis C virus nonstructural protein 5A (NS5A) is an RNA-binding protein. *J. Biol. Chem.* **280**, 36417–36428 (2005).
35. Roosild, T.P. *et al.* NMR structure of Mistic, a membrane-integrating protein for membrane protein expression. *Science* **307**, 1317–1321 (2005).
36. Schilders, G., Raijmakers, R., Raats, J.M.H. & Pruijn, G.J.M. MPP6 is an exosome-associated RNA-binding protein involved in 5.8S rRNA maturation. *Nucleic Acids Res.* **33**, 6795–6804 (2005).